Research Square

Preprints are preliminary reports that have not undergone peer review.
They should not be considered conclusive, used to inform clinical practice,
or referenced by the media as validated information.

Comparison of Susceptibility Artifacts of Dental Materials in Magnetic Resonance Imaging According to Different Sequences

Nazan Kocak Topbas

nazannkocak@gmail.com

Mersin University

Aynur Korkmaz

Mersin University

Songül Barlaz Us

Mersin University

Kıvanc Kamburoglu

Feramuz Demir Apaydın

Mersin University

Article

Keywords: Magnetic resonance imaging, dental materials, magnetic susceptibility artifacts, artifact reduction techniques

Posted Date: June 5th, 2026

DOI: https://doi.org/10.21203/rs.3.rs-9791923/v1

License: This work is licensed under a Creative Commons Attribution 4.0 International License.
Read Full License

Additional Declarations: No competing interests reported.

Abstract

Magnetic susceptibility artifacts caused by dental materials may significantly degrade magnetic resonance imaging (MRI) quality and hinder accurate diagnostic interpretation. This study aimed to compare the extent of artifacts produced by commonly used dental materials with different magnetic properties across multiple MRI sequences. Human cadaveric dry jawbones were used to construct a phantom containing eight dental materials representing ferromagnetic, paramagnetic, and diamagnetic characteristics. Imaging was performed using a 3T MRI system with T1-weighted and T2-weighted Turbo Spin Echo sequences and their corresponding View Angle Tilting (VAT) modifications. Artifact areas were quantitatively assessed on standardized coronal slices by manually delineating regions encompassing both signal void and hyperintense distortion zones surrounding each material. Statistical analysis was conducted using one-way ANOVA followed by Tukey post hoc tests, with significance set at $p < 0.05$. Ferromagnetic materials generated the largest artifacts and caused marked anatomical distortion, whereas paramagnetic materials also produced substantial artifacts, particularly around implant abutments. Diamagnetic materials exhibited minimal or negligible artifact formation. T2-weighted sequences demonstrated greater susceptibility to artifacts compared with T1-weighted sequences. The VAT technique reduced artifact size but did not fully eliminate distortion. Overall, artifact severity was strongly dependent on the magnetic properties of dental materials and the imaging sequence used. Although VAT improved image quality, advanced metal artifact reduction techniques such as Slice Encoding for Metal Artifact Correction (SEMAC) may provide further benefits in clinical imaging of patients with dental restorations.

Introduction

Magnetic Resonance Imaging (MRI) stands out as a leading non-invasive diagnostic tool, delivering exceptional soft tissue contrast and multiplanar views without the risks associated with ionizing radiation. Although Computed Tomography (CT) and Cone-Beam Computed Tomography (CBCT) are widely used in maxillofacial imaging, MRI's superior contrast-to-noise ratio (CNR) for soft tissues has made it the gold standard for evaluating complex orofacial conditions [1]. Advances in gradient coil technology and pulse sequence refinement have expanded MRI's role from primarily neuroimaging to routine clinical use in dentistry [2–5]. The diagnostic power of MRI depends on signal intensity (SI), which varies with tissue relaxation properties. Areas appearing bright are described as hyperintense, while darker regions are hypointense. These signal patterns relate closely to the pulse sequences used for example, T1-weighted (T1w) sequences highlight fat and paramagnetic substances like gadolinium contrast with high SI, while fluids such as cerebrospinal fluid (CSF) show low signal [6]. T2-weighted (T2w) sequences emphasize pathological changes like edema, inflammation, or tumors, which typically appear bright, whereas the fat signal diminishes compared to T1w images [7]. Bone cortex and air consistently appear dark due to low proton density and rapid signal decay, but fatty marrow within cancellous bone shows high SI on T1w and intermediate SI on T2w images [7].

Despite these strengths, MRI in the maxillofacial region faces challenges from dental materials such as endodontic fillers, crowns, and titanium implants that cause magnetic susceptibility mismatches at the tissue-material interface. Ferromagnetic alloys, in particular, disrupt the static magnetic field (B_0), creating signal voids, spatial distortions, and hyperintense artifact pile-ups [8,9]. These artifacts degrade image quality and obscure critical anatomical details, risking misdiagnosis [10]. Understanding how these artifacts vary across pulse sequences like Spin Echo (SE) and Gradient Recalled Echo (GRE) is essential to tailor MRI protocols for patients with dental hardware.

As diverse dental materials become more common, it is vital to assess their impact on high-field MRI. Although 3T MRI offers clinical advantages, susceptibility artifacts manifesting as signal loss and distortion remain a major barrier to clear imaging in the maxillofacial region [11]. Previous studies evaluating MRI artifacts caused by dental materials have mainly focused on specific appliances, a limited range of dental materials, or limited MRI protocols [12–17]. Although advanced metal artifact reduction techniques such as PETRA, SEMAC, and VAT-enhanced sequences have shown promising results in reducing susceptibility artifacts [4,17], comparative quantitative analyses involving multiple commonly used dental materials across both conventional and VAT-supported TSE sequences at 3T MRI remain limited [15,16]. Therefore, this study aimed to quantitatively compare artifact sizes caused by eight frequently used dental materials across four MRI sequences: T1-weighted Turbo Spin Echo (T1-TSE), T2-weighted Turbo Spin Echo (T2-TSE), and their View Angle Tilting (VAT)-enhanced versions (T1-TSE-VAT and T2-TSE-VAT). Identifying the sequences least affected by these artifacts may help optimize clinical MRI protocols and improve diagnostic accuracy in patients with metallic or non-metallic dental restorations.

Results

Observer Agreement

In MRI measurements, excellent intraobserver agreement was observed for both observers. The ICC values were 0.946 (95% CI: 0.901–0.972) for Observer 1 and 0.934 (95% CI: 0.884–0.962) for Observer 2. All agreement analyses demonstrated statistically significant reliability ($p < 0.05$).

Artifact Area Analysis

Figure 3 shows coronal plane MR images of dental materials placed in dry human cadaver jaws, illustrating their distribution and artifact appearances across the four sequences.

The mean values and standard deviations of the hyperintense and hypointense artifact areas of different dental materials across four MR sequences (T2-TSE, T2-TSE-VAT, T1-TSE, and T1-TSE-VAT) are presented in Table 3. Significant differences were found among sequences for amalgam, metal crown, implant abutment, orthodontic bracket, and calcium hydroxide medicament ($p < 0.05$).

Table 3
Mean artifact areas and standard deviations of dental materials on MR images across different sequences

Amalgam	**T1-TSE**	**T1-TSE-VAT**	**T2-TSE**	**T2-TSE-VAT**
	0,895 ± 0,004^{b,c,d}	**0,776 ± 0,002^{a,c,d}**	**1,459 ± 0,021^{a,b,d}**	**0,918 ± 0,005^{a,b,c}**
Composite	1,004 ± 0,004^{b,c}	1,028 ± 0,004^{a,c,d}	0,932 ± 0,002^{a,b,d}	1,0003 ± 0,002^{b,c}
Metal Crown	3,017 ± 0,008^{b,c,d}	2,51 ± 0,015^{a,c,d}	3,35 ± 0,016^{a,b,d}	2,37 ± 0,004^{a,b,c}
Implant Abutment	1,992 ± 0,011^{b,,c,d}	1,536 ± 0,07 ^{a,c,d}	2,454 ± 0,042 ^{a,b,d}	1,676 ± 0,021 ^{a,b,c}
GIC	0,516 ± 0,001^{b,d}	0,505 ± 0,004^{a,c,d}	0,516 ± 0,001^{b,d}	0,4507 ± 0,001^{a,b,c}
Bracket	13,386 ± 0,055 ^{b,c,d}	8,814 ± 0,004 ^{a,c,d}	15,44 ± 0,065 ^{a,b,d}	8,346 ± 0,052 ^{a,b,c}
Endodontic fiiling	0,267 ± 0,001^{b,d}	0,216 ± 0,003^{a,c,d}	0,265 ± 0,002^{b,d}	0,263 ± 0,002^{a,b,c}
$Ca(OH)_2$ Medicament	0,163 ± 0,003^{b,,c,d}	0,151 ± 0,0005 ^{a,c,d}	0,256 ± 0,003^{a,b,d}	0,187 ± 0,003 ^{a,b,c}
Implant Body	0,356 ± 0,004 ^{b,d}	0,174 ± 0,002 ^{a,c,d}	0,364 ± 0,039 ^{b,d}	0,23 ± 0,001 ^{a,b,c}
a: different from T1-TSE, b: different from T1-TSE-VAT, c: different from T2-TSE, d: different from T2-TSE-VAT				

For composite material, no significant difference existed between T2-TSE-VAT and T1-TSE ($p > 0.05$), but other sequence comparisons showed significant differences ($p < 0.05$).

In endodontically treated tooth, significant differences were noted between T2-TSE and T2-TSE-VAT, and between T2-TSE and T1-TSE. A borderline difference was observed between T2-TSE-VAT and T1-TSE ($p = 0.052$). In the glass ionomer cement (GIC) filling and implant body regions, no significant difference was observed between T2-TSE and T1-TSE; however, significant differences were found in the other pairwise comparisons ($p < 0.05$).

Discussion

This study offers a detailed evaluation of magnetic susceptibility artifacts caused by common dental materials. Artifact severity depends mainly on the materials' magnetic properties and alloy composition. Ferromagnetic materials produced the largest artifacts, followed by paramagnetic materials, while diamagnetic materials had minimal impact on image quality.

Ferromagnetic substances like stainless steel brackets and nickel–chromium crowns caused extensive signal voids and distortions, often obscuring anatomical details entirely. This reflects their strong magnetic interaction, disrupting the local magnetic field. These results align well with previous studies [12–14], confirming ferromagnetic dental components as a major MRI limitation in head and neck imaging. Notably, artifacts were more pronounced in T2-weighted sequences, suggesting that susceptibility effects vary by sequence and should guide protocol choices. Nevertheless, inconsistencies with prior studies [15,16] highlight that artifact behavior cannot be generalized and is highly sensitive to scanner-specific parameters, including field strength and sequence design.

VAT sequences reduced artifact size somewhat, but not enough to restore diagnostic image quality near ferromagnetic materials. Persistent signal loss and geometric distortion, even after VAT application, underscore the inherent limitations of this technique when used in isolation. This is consistent with previous reports [17], which emphasize that advanced multi-slice correction strategies such as SEMAC are required for substantial artifact mitigation. From a clinical perspective, these findings suggest that reliance on VAT alone may be inadequate in cases involving ferromagnetic dental hardware and combined or alternative artifact-reduction approaches should be considered.

In contrast, paramagnetic materials demonstrated a more moderate impact on MR image quality, characterized by localized hypointense regions and limited hyperintense signal accumulation. Nevertheless, the observation that implant abutments generated more pronounced artifacts than amalgam despite both being classified as paramagnetic highlights the critical influence of alloy composition and trace ferromagnetic content. This finding is particularly relevant given the widespread clinical use of titanium-based implants. Although titanium is generally regarded as a non-ferromagnetic material and is therefore expected to produce minimal artifacts in MR imaging, the literature presents conflicting evidence. Some studies have reported that titanium induces only small-scale artifacts that do not significantly compromise image quality [18,19]. Conversely, Costa et al. [20], in a retrospective evaluation of brain MR images in patients with epilepsy, suggested that titanium implants may contain trace amounts of ferromagnetic iron, potentially leading to clinically relevant susceptibility artifacts. Therefore, the assumption that all titanium-based materials are artifact-free should be approached with caution.

The inability to clearly delineate root canal boundaries and the implant body further emphasizes the limitations of MRI in regions characterized by low proton density tissues. The inherently low signal from mineralized dental tissues, combined with susceptibility effects, creates a challenging imaging environment in which both anatomical detail and material interfaces may be obscured. This limitation is not solely related to material properties but also reflects fundamental constraints of MR signal generation in hard tissues.

Diamagnetic materials exhibited negligible artifact formation across all evaluated sequences, confirming their minimal interaction with the magnetic field. The absence of significant distortions supports their suitability in clinical scenarios where MR imaging is anticipated. Minor signal variations observed in

these materials are likely attributable to structural heterogeneity rather than true susceptibility effects. These findings are consistent with prior reports [8,21,22] and reinforce the clinical advantage of using diamagnetic restorative materials in patients who may require MR imaging.

From a methodological standpoint, the observed variability in statistical significance across sequences highlights the sensitivity of quantitative artifact assessment to factors such as ROI placement and measurement precision, particularly in small-volume regions. This underscores the importance of standardized measurement protocols and, where possible, automated or semi-automated segmentation techniques to improve reproducibility. Clinically, these findings emphasize that dental material selection should consider MRI compatibility alongside mechanical and esthetic properties. MRI protocols for patients with dental restorations should incorporate advanced artifact reduction techniques when feasible. Overall, magnetic susceptibility artifacts are strongly dependent on the magnetic properties and composition of dental materials, with ferromagnetic materials producing the most severe distortions, paramagnetic materials causing moderate artifacts, and diamagnetic materials showing negligible effects. Although VAT-based techniques provide partial reduction of artifacts, they remain insufficient for correcting severe distortions, particularly those caused by ferromagnetic materials, highlighting the need for advanced approaches such as SEMAC. These results also indicate that even materials commonly regarded as MRI-compatible, such as titanium-based alloys, may still generate clinically relevant artifacts depending on their composition. Future research should focus on combined artifact reduction strategies and their performance across different imaging conditions to improve diagnostic reliability.

Materials and Methods

Ethical Approval

and Sample Selection

This in vitro study was conducted following approval from the Mersin University Clinical Research Ethics Committee (Decision No: 1093; 13 November 2024) and in accordance with institutional ethical guidelines and the principles outlined in the Declaration of Helsinki.

Prior to the study, sample size estimation was performed using G*Power software (version 3.1.9.6) to ensure adequate statistical power for comparisons among the investigated dental materials. The power analysis indicated that a minimum sample size of eight specimens would be sufficient to detect statistically significant differences with a statistical power of 95% and a significance level of 5%.

Human cadaveric dry maxillary and mandibular jawbones were used to create the experimental model. Seven dental materials frequently encountered in clinical practice were evaluated using premolar and molar teeth prepared with the respective restorative or endodontic applications. In addition, a dental implant body with its corresponding abutment was included as a separate test specimen (Table 1).

Table 1
Dental materials used in the study and their composition

Dental Material	Composition
Composite	Barium silicate, organic-inorganic fillers, Bis-GMA, dl-camphorquinone (Clearfil Majesty Esthetic, Japan)
Amalgam	50% Mercury (Hg), 45% Silver (Ag), Tin (Sn), Copper (Cu), Zinc (Zn)
Glass Ionomer Cement	Silicate glass powder, polyalkenoic acid (Imicryl Nova Glass F, USA)
Calcium Hydroxide Medicament	48% Calcium hydroxide ($CaOH_2$), barium sulfate, silicone oil (RC Cal-Prime Dental, India)
AH Plus Root Canal Sealer / Gutta-percha (Endodontic fiiling)	Epoxy-amine resin (Dentsply, Germany)/ Polyisoprene rubber, zinc oxide, barium sulfate (Pearl Endo, Vietnam)
Metal Crown Restoration	Nickel (60%), Chromium (20–30%) dental alloy
Implant Body Implant Abutment	Titanium alloy (Titanium (Ti), Aluminum (Al), Vanadium (V)) (Mode Implant, Türkiye)
Bracket	Stainless steel bracket (65–70% Iron (Fe), 17–20% Chromium (Cr), 8–10% Nickel (Ni)) (Rocky Mountain Orthodontics, USA)

The investigated materials consisted of composite resin, amalgam, glass ionomer cement, metal crowns, orthodontic brackets, calcium hydroxide intracanal medicament, and root canal filling material composed of gutta-percha and AH Plus sealer. A non-restored intact tooth without caries, fractures, or anatomical irregularities was used as the control sample.

Specimens were distributed randomly into preserved alveolar sockets, with each jaw containing only one material configuration to avoid overlap of susceptibility artifacts between adjacent regions. Jaw specimens presenting fractures, structural deformities, socket deficiencies, or unstable tooth positioning were excluded from the study.

Phantom Preparation

To simulate soft-tissue conditions encountered in clinical imaging, the outer surfaces of the jaw specimens were covered with a layer of paraffin wax. Subsequently, the specimens were positioned within rectangular plastic containers and embedded in a homogeneous mixture of water and bovine gelatin to reproduce soft-tissue signal characteristics during MRI acquisition (Fig. 1).

The prepared phantoms were allowed to stabilize overnight at room temperature until complete solidification was achieved. To maintain consistent positioning throughout image acquisition, all phantoms were oriented using the same spatial arrangement within the imaging container.

Imaging Protocol

MRI scans were performed on a 3T Siemens Magnetom Vida scanner (Erlangen, Germany). Four sequences were applied with acquisition parameters listed in Table 2. Phantoms were positioned in a dedicated head coil and stabilized with foam sponges to avoid motion artifacts.

Table 2
MRI sequences and acquisition parameters used in this study

Eco Time (TE)(ms)	**T1-TSE**	**T1-TSE-VAT**	**T2-TSE**	**T2-TSE-VAT**
	8.50	**7.80**	**100**	**99**
Repetition Time (TR)(ms)	726	677	4750	4210
Matrix Size	192/256	192/256	192/256	192/256
FOV (mm)	220	220	220	220
Slice Thickness (mm)	2	2	2	2
Inter-slice Gap	1	1	1	1

Radiological Image Analysis

Artifact Scoring and Slice Selection

MRI datasets were exported in DICOM format for image analysis (Fig. 2). All images were independently assessed by two experienced dentomaxillofacial radiologists. For each dental material and imaging sequence, the anatomical region containing the most prominent artifact expression was initially identified within the volumetric dataset.

Within the selected region, artifact severity was graded using a five-point scale ranging from 1 (minimal artifact) to 5 (severe artifact). After independent evaluation, both observers reached a consensus regarding the slice demonstrating the maximum visible artifact extent. The corresponding coronal slice was subsequently selected for quantitative artifact analysis.

To maintain consistency between sequence comparisons, the same anatomical slice level was used for evaluation of T1-TSE, T1-TSE-VAT, T2-TSE, and T2-TSE-VAT images. The identical procedure was also applied to the control tooth images.

Artifact Area Quantification

The selected MRI slices were analyzed using RadiAnt DICOM Viewer software (Medixant Ltd., Poznan, Poland). Artifact measurements were performed using the “Closed Polygon ROI” tool. For each image, the visible boundaries of the artifact surrounding the dental material were manually delineated, including both hypointense signal void regions and adjacent hyperintense signal pile-up areas. Following manual segmentation, the software automatically calculated the total artifact area in square millimeters (mm^2). To ensure standardized measurements, all delineations were performed under identical magnification and display conditions.

All measurements were independently performed by both observers. To evaluate intraobserver reproducibility, 50% of the images were randomly re-evaluated by the same observers after an interval of approximately three weeks. Inter- and intraobserver agreement were assessed using the Intraclass Correlation Coefficient (ICC). For statistical analysis, the mean of both observers’ measurements was used.

Statistical Analysis

Statistical analysis was conducted with SPSS v25.0 (IBM Corp., NY, USA). The normality of the data distribution was confirmed via homogeneity testing. Differences among the groups were analyzed using One-Way Analysis of Variance (ANOVA), followed by the Tukey post hoc test for multiple comparisons. The threshold for statistical significance was set at $p < 0.05$.

Inter- and intraobserver reliability for artifact area measurements were evaluated using the Intraclass Correlation Coefficient (ICC) based on a two-way random-effects model with absolute agreement.

Declarations

Ethics approval and consent to participate

This in vitro study was conducted in accordance with the ethical principles of the Declaration of Helsinki and was approved by the Clinical Research Ethics Committee of Mersin University (Decision No: 1093, Date: 13 November 2024). As the study used extracted human teeth and dry human jaws obtained in accordance with institutional and national regulations, informed consent to participate was waived by the Ethics Committee, as no living human participants or identifiable personal data were involved.

Acknowledgements

The authors gratefully acknowledge the radiology technicians for their assistance during the CBCT imaging procedures.

Author Contributions

A.K., N.K.T., S.B.U. and K.K. contributed to conceptualization.
A.K., N.K.T., S.B.U., K.K. and F.D.A. contributed to methodology.
A.K., N.K.T. and S.B.U. contributed to investigation.
A.K., N.K.T. and S.B.U. contributed to formal analysis.
A.K. and N.K.T. contributed to writing – original draft.
N.K.T., S.B.U. and K.K. contributed to writing – review & editing.
N.K.T., S.B.U., K.K. and F.D.A. contributed to supervision.

Data Availability Statement

The datasets generated and analysed during the current study are available from the corresponding author on reasonable request.

Competing Interests

The authors declare no competing interests.

Consent for publication

Not applicable.

Funding

No funding was obtained fort his study.

References

1. Korn P, Elschner C, Schulz M, Range U, Mai R, Scheler U. MRI and dental implantology: two which do not exclude each other. *Biomaterials*. 2015;53:634–645. https://doi.org/10.1016/j.biomaterials.2015.02.114
2. Flügge T, et al. Magnetic resonance imaging of intraoral hard and soft tissues using an intraoral coil and FLASH sequences. *Eur Radiol*. 2016;26:4616–4623. https://doi.org/10.1007/s00330-016-4254-1
3. Prager M, Heiland S, Gareis D, Hilgenfeld T, Bendszus M, Gaudino C. Dental MRI using a dedicated RF-coil at 3 Tesla. *J Cranio-Maxillofac Surg*. 2015;43:2175–2182. https://doi.org/10.1016/j.jcms.2015.10.011
4. Hilgenfeld T, et al. PETRA, MSVAT-SPACE and SEMAC sequences for metal artefact reduction in dental MR imaging. *Eur Radiol*. 2017;27:5104–5112. https://doi.org/10.1007/s00330-017-4901-1
5. Tutton L, Goddard P. MRI of the teeth. *Br J Radiol*. 2002;75:552–562. https://doi.org/10.1259/bjr.75.894.750552
6. Xiao Y-D, Paudel R, Liu J, Ma C, Zhang Z-S, Zhou S-K. MRI contrast agents: Classification and application (Review). *Int J Mol Med*. 2016;38:1319–1326. https://doi.org/10.3892/ijmm.2016.2744

7. Sprawls P. Magnetic resonance imaging: principles, methods, and techniques. Madison: Medical Physics Publishing; 2000.
8. Tymofiyeva O, et al. Influence of dental materials on dental MRI. *Dentomaxillofac Radiol*. 2013;42:20120271. https://doi.org/10.1259/dmfr.20120271
9. Hargreaves BA, Worters PW, Pauly KB, Pauly JM, Koch KM, Gold GE. Metal-induced artifacts in MRI. *AJR Am J Roentgenol*. 2011;197:547–555. https://doi.org/10.2214/AJR.11.7364
10. 10. Bohner L, Hanisch M, Sesma N, Blanck-Lubarsch M, Kleinheinz J. Artifacts in magnetic resonance imaging caused by dental materials: a systematic review. *Dentomaxillofac Radiol*. 2022;51:20210450. https://doi.org/10.1259/dmfr.20210450
11. Latzko L, Schmit A, Glodny B, Grams AE, Birkl C, Crismani AG. Orthodontic appliances and their diagnostic impact to brain MRI. *Clin Oral Investig.* 2025;29(4):202. https://doi.org/10.1007/s00784-025-06275-8
12. Cassetta M, et al. The effects of a common stainless steel orthodontic bracket on the diagnostic quality of cranial and cervical 3T-MR images: a prospective, case-control study. *Dentomaxillofac Radiol*. 2017;46:20170051. https://doi.org/10.1259/dmfr.20170051
13. Elison JM, Leggitt VL, Thomson M, Oyoyo U, Wycliffe ND. Influence of common orthodontic appliances on the diagnostic quality of cranial magnetic resonance images. *Am J Orthod Dentofacial Orthop*. 2008;134:563–572. https://doi.org/10.1016/j.ajodo.2006.10.038
14. Hinshaw D Jr, Holshouser B, Engstrom H, Tjan A, Christiansen E, Catelli W. Dental material artifacts on MR images. *Radiology*. 1988;166:777–779. https://doi.org/10.1148/radiology.166.3.3340777
15. Valizadeh S, Pouraliakbar H, Arzani V, Nahardani A. Quantification of artifacts in MR images caused by commonly used dental materials. *Iran J Radiol*. 2017;14:1–10. https://doi.org/10.5812/iranjradiol.55566
16. Kocasarac HD, et al. Evaluation of artifacts generated by titanium, zirconium, and titanium–zirconium alloy dental implants on MRI, CT, and CBCT images: A phantom study. *Oral Surg Oral Med Oral Pathol Oral Radiol*. 2019;127:535–544. https://doi.org/10.1016/j.oooo.2019.01.074
17. Zho SY, Kim MO, Lee KW, Kim DH. Artifact reduction from metallic dental materials in T1-weighted spin-echo imaging at 3.0 tesla. *J Magn Reson Imaging*. 2013;37:471–478. https://doi.org/10.1002/jmri.23785
18. Holton A, Walsh E, Anayiotos A, Pohost G, Venugopalan R. Comparative MRI compatibility of 316L stainless steel alloy and nickel–titanium alloy stents: original article technical. *J Cardiovasc Magn Reson*. 2002;4:423–430.
19. Fache JS, Price C, Hawbolt EB, Li D. MR imaging artifacts produced by dental materials. *AJNR Am J Neuroradiol*. 1987;8:837–840.
20. Costa ALF, Appenzeller S, Yasuda CL, Pereira FRS, Zanardi VA, Cendes F. Artifacts in brain magnetic resonance imaging due to metallic dental objects. 2009.
21. Gowda E, Sahoo N. MRI compatibility of dental materials. Int J Med Sci Adv Clin Res. 2020;3(4):19–24.

22. Grosse U, et al. Magnetic resonance imaging of solid dental restoration materials using 3D UTE sequences: visualization and relaxometry of various compounds. *Magn Reson Mater Phys Biol Med*. 2013;26:555–564. https://doi.org/10.1007/s10334-013-0373-8

Figures



Figure 1

Phantom preperation

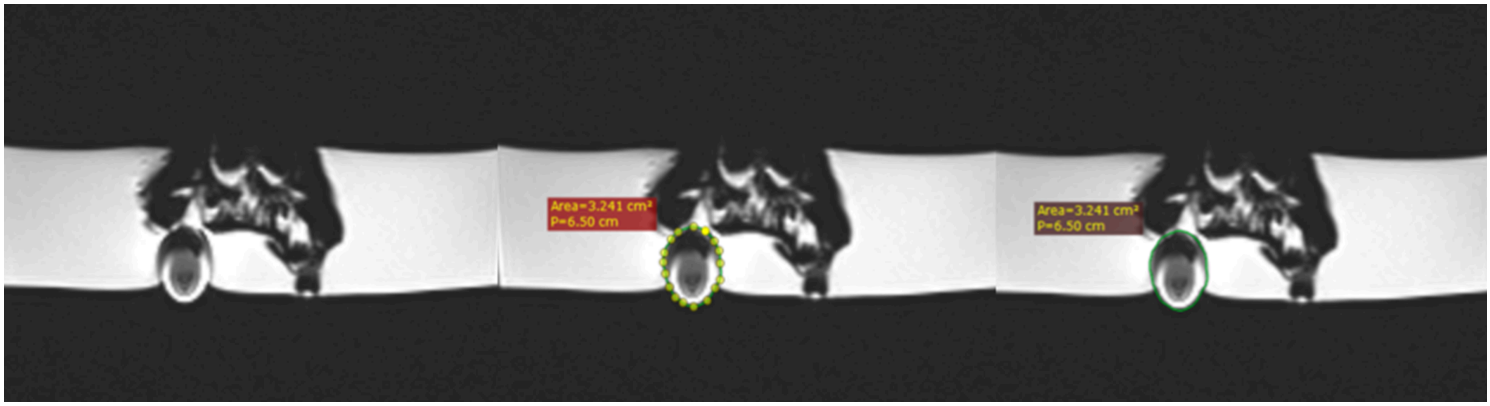


Figure 2

Stepwise demonstration of artifact area measurement on MR images using the closed polygon ROI tool. From left to right: (A) original coronal slice showing metal-induced artifacts, (B) manual delineation of artifact boundaries including both hypointense and hyperintense regions using the polygon ROI tool, and (C) final ROI with calculated area (cm^2) and perimeter (cm)

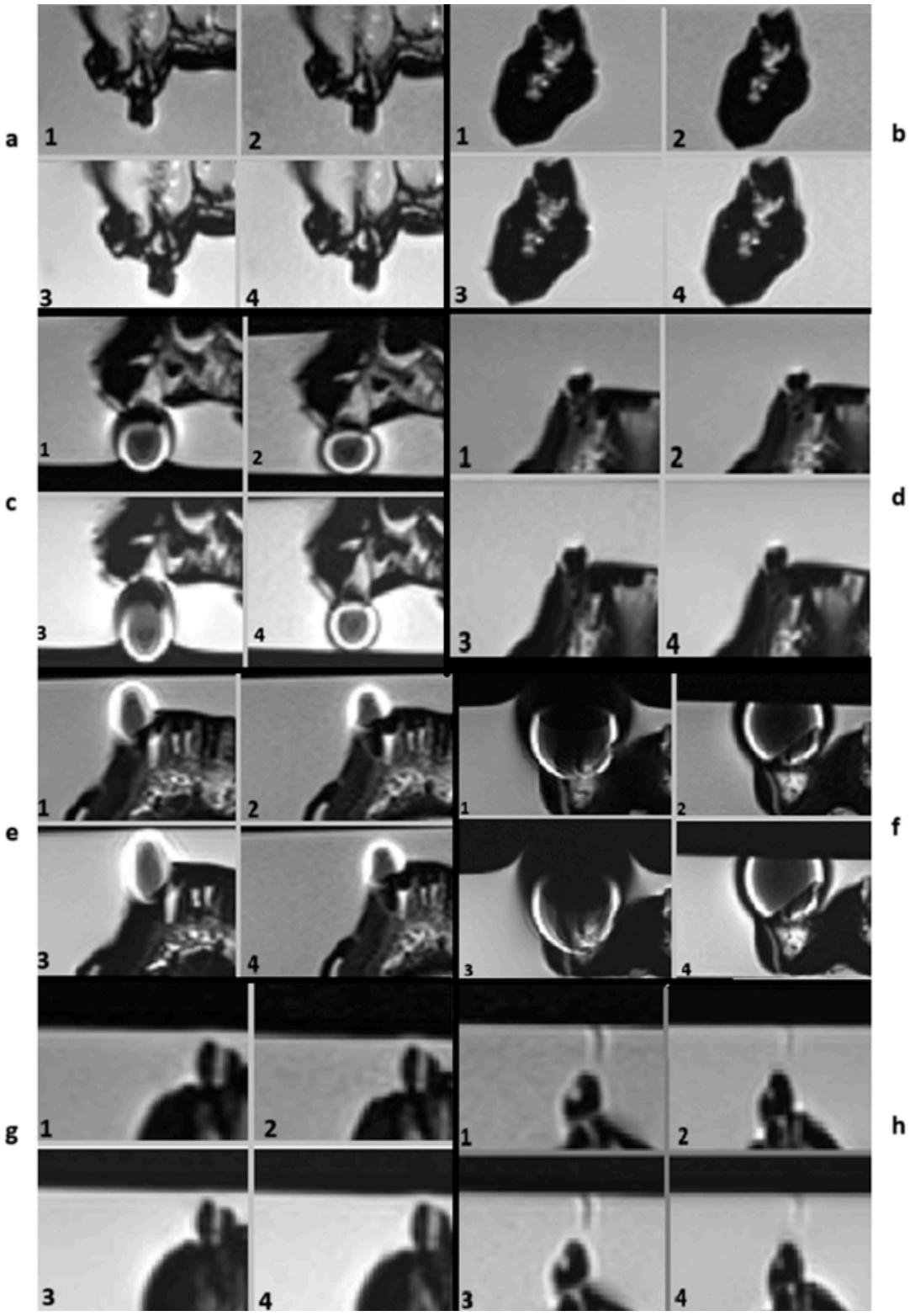


Figure 3

MR images of dental materials placed in the jaws of a dry human cadaver, shown in coronal sections across four different sequences: (a) Amalgam, (b) Composite, (c) Metal crown, (d) GIC restoration, (e) Implant abutment, (f) Orthodontic bracket, (g) Endodontic filling, (h) Calcium hydroxide medication; sequences: 1: T1-TSE, 2: T1-TSE-VAT, 3: T2-TSE, 4: T2-TSE-VAT